NASA Technical Memorandum 82953

Measurements of Self-excited Rotor-blade Vibrations Using Optical Displacements

A. P. Kurkov
Lewis Research Center
Cleveland, Ohio

Prepared for the
Twenty-eighth Annual International Gas Turbine Conference
sponsored by the American Society of Mechanical Engineers
Phoenix, Arizona, March 27-31, 1983

NASA

MEASUREMENTS OF SELF-EXCITED ROTOR-BLADE VIBRATIONS USING OPTICAL DISPLACEMENTS

A. P. Kurkov

National Aeronautics and Space Administration
Lewis Research Center
Cleveland, Ohio 44135

ABSTRACT

During the operation of a turbofan engine at part speed, near stall, and elevated inlet pressure and temperature, several vibratory instabilities were excited simultaneously on the first fan rotor. The torsional and bending contributions to the main flutter mode were resolved by using casing-mounted optical displacement sensors. Strain-gage spectra were used to identify other instabilities in the blade-deflection spectra. The characteristics of optical-displacement spectra and their role of monitoring rotor-blade vibrations are discussed.

NOMENCLATURE

A = amplitude
a = port separation along the chord, Fig. 1
c = blade chord
D = total tangential displacement
d = displacement component of D
h = bending displacement, Fig. 1
j = imaginary unit
k = revolution counter
l = blade counter
n = number of revolutions
Q = number of points per revolution
q = point-per-revolution counter
r = radial coordinate, Fig. 1
γ = stagger angle, Fig. 1
θ = angular displacement, Fig. 1
ϕ = angular coordinate in rotating frame of reference
ϕ = phase angle
ω = circular frequency

Subscripts:
f = flutter
h = bending
i = nodal diameter
l = leading edge port
m = midchord port
r = rotational
s = strain gage
t = trailing-edge port
u = unsteady component
θ = torsion

INTRODUCTION

Turbomachinery vibrations can be classified either as forced vibrations, which occur in response to stationary upstream or downstream disturbances, or as self-excited vibrations for which no obvious source of excitition is present. Self-excited vibrations are usually associated with either the individual blade natural frequencies or a rotor-assembly natural frequency. In general, therefore, these vibrations occur at a nonintegral multiple of rotational frequency.

Flutter is the most frequent and best documented self-excited vibration. All blades in flutter vibrate at the same frequency and the phase angle between the two consequtive blades (i.e., interblade phase angle) is well defined. Thus, in a rotating frame of reference, flutter can be described by a traveling wave. However, the amplitudes and interblade phase angles do not necessarily have to be uniform around the rotor. In such a case several traveling waves are present simultaneously. This occurs, for example, when the single-blade natural frequencies are not all identical; that is, when rotor blades are mistuned (1).

Stationary optical sensors are well suited for displacement measurements during flutter or during any other self-excited vibration at a nonintegral multiple of rotational frequency. Optical sensors were discussed in (2) and the quantitative analysis methods in (3-5). This paper presents results for a more complicated situation. Several vibratory modes were excited simultaneously, and flutter occurred in a second coupled mode which involves both bending and torsional blade displacements. (In (3-5) the vibratory mode was first torsion and no other excititions were present.) This paper is primarily intended to illustrate the capabilities and limitations of the optical displacement measurements and to illustrate the analysis procedure for

this complex multiple-mode excitition. However, certain results are also expected to be of more general interest.

The instabilities described in this paper (and in (3-5)) occurred in the first fan rotor during part-speed, near-stall operation at elevated inlet pressure and temperature. For the particular test point discussed herein, a tip-radial screen was installed in the inlet duct. The blade-tip relative Mach number was 0.954 and the reduced frequency (based on the blade chord) at the tip span was 1.39. The fan blades were equipped with shrouds at 54 percent of the span.

Personnel at Pratt and Whitney Aircraft, Government Products Division, and in particular Mr. A. W. Stoner is credited for obtaining the estimates for blade deflections, the streamline blade-element parameters, and the single blade holograms.

EXPERIMENTAL MEASUREMENTS AND DATA PROCESSING

Only a brief description of optical displacements measurements is given in this paper since a detailed description is reported in (2). Figure 1 illustrates the position of optical ports in the engine casing relative to a rotor blade. As the blades passed optical ports, a light beam was reflected from the blade tips and conducted to a photomultiplier by a fiber-optics bundle. A voltage pulse was generated every time a blade passed an optical port. The position of this pulse relative to the once-per-revolution (1E) signal indicated the instanteneous position of a blade in flutter. The blade pulses and the reference 1E signal were recorded at 304.8 cm/s (120 in/s) on a wideband I FM tape recorder.

During the postrun analysis, the tape was played back at 1/64 of the recording speed, and the two channels of data (a once-per-blade pulse train generated by the optical sensor and the once-per-revolution reference signal) were digitized at the maximum possible rate (20,480 Hz/channel). The resulting resolution (about 8860 points/revolution) was sufficient to capture the blade motion corresponding to main flutter mode. However, to capture some of the smaller displacement associated with higher modes, it was desirable to attain a higher resolution. This could only be achieved by reducing the signal frequency further during playback. Since no further reduction of the tape speed was possible, the data were recorded on another tape at four times the speed of the original tape. Thus, four times higher resolution could be achieved during playback. However, experimentation showed that doubling the original resolution was sufficient. Therefore, the number of points per revolution during the data analysis was 17,720.

One difficulty encountered during this procedure was the loss of precise synchronization between the displacement and the strain-gage tapes. It was intended to achieve this synchronization by using the time code signal recorded on all tapes. However, because the resulting frequency of the time code signal during playback was too low, it could not be read. Since the channel to channel synchronization depended on using the time code signal, another time code had to be recorded on the second FM tape. (In this procedure (3-5) the data acquisition is initiated at the first 1E pulse after the preselected time instant is read from the tape.)

In this analysis the 1E reference pulse is used rather than the once per blade as in (3-5). Therefore, when instantaneous blade positions were computed, a correction was applied to compensate for the slight variation in speed (and thus in the count per revolution) during the sampling interval. The compensation is accomplished by multiplying the instantaneous pulse positions by the ratio of the average count per revolution by the current count per revolution. This correction was not necessary when the once-per-blade reference was used (3-5) because of the closeness of the reference pulse to the blade pulse.

One problem encountered in triggering blade pulse signals, particularly for the leading and trailing edge ports, was the uneven pulse height. This problem was solved by assigning trigger levels based on blade pulse heights. The levels were derived from the averaged (each point q, q = 1,...,Q, is averaged over n revolutions) pulse-train distribution, which was also used to derive a window for each blade. The search for a trigger was performed only in the immediate vicinity (i.e., window) of the particular blade pulse to avoid triggering on a spurious signal. In case a pulse was missing, its average trigger position (obtained from triggering the averaged distribution) was substituted.

As in (3-5), removing of the DC displacement component for each blade l to obtain the unsteady instanteneous tangential dislacements is accomplished by using

$$D_u(l,k) = D(l,k) - (1/n) \sum_{k=1}^{n} D(l,k),$$

$$l = 1,\ldots,N \quad k = 1,\ldots,n \qquad (1)$$

The spectral analysis is performed for either a set of points k = 1,...,n for each blade l (i.e., individual blade spectra) or a set of points l = 1,...,N,k = 1; l = 1,...,N,k = 2;...(i.e., overall spectrum). Because Singleton's (5) algorithm was used to obtain the spectra, neither set of points was restricted to a power of two points.

In a rotating frame of reference, flutter vibrations can be described (4,5) by a summation of waves:

$$D = \sum_{i=1}^{N} A_i \cos(\omega_f t - i\phi + \phi_i) \qquad (2)$$

where time t and angular coordinate ϕ (positive in the direction of rotation) are independent variables. However, from the point of view of a stationary sensor, ϕ is not arbitrary but equal to $-\omega_r t$. Thus, the signal received by a stationary sensor becomes

$$D = \sum_{i=1}^{N} A_i \cos[(\omega_f + \omega_r i)t + \phi_i] \qquad (3)$$

and each constituent wave is shifted in frequency by $\omega_r i$.

ANALYSIS OF THE RESULTS

Strain-Gage and Overall-Displacement Spectra

The analysis of the blade deflection data for this engine is complicated by the fact that several non-integral engine order modes with widely different frequencies were excited simultaneously. This is il-

lustrated by the strain-gage spectra (Figs. 2-4). The strain gages were located close to the blade tip and about 31 percent of the chord from the leading edge. The highest stress levels for nonintegral engine order frequencies were observed at 5.159, 10.319 E, and around 14-16E. (The frequencies are presented in engine orders to clearly distinguish the integral and nonintegral engine-order responses and for convenience when correlating different peaks in the strain-gage and displacement spectra. One engine order corresponded to 147.7 Hz.)

The 5.159 E frequency corresponds to the second coupled mode family. In this mode both bending and torsional deflections are significant. It can be seen that 10.319 E frequency is nearly twice 5.159 E. It appears, therefore, that 10.319 E response is the second harmonic of the coupled flutter mode. However, as will be seen, the lack of response in the displacement spectra at this frequency indicates that motion at this frequency corresponds to a higher mode. Based on a single-blade hologram, 10.319 E is very near the above-shroud second bending mode frequency. The response at this frequency will, therefore, be considered as a separate mode. Note, however, that the factor of two difference with the 5.159 E frequency indicates a possible nonlinear coupling between these two responses. The frequencies in the 14-16E band are most closely associated with the above-shroud chordwise bending mode. (Most are 100 to 200 Hz lower than the frequency corresponding to this mode.)

In contrast to the strain-gage spectra, the overall tip-diplacement spectra (Figs. 5-7) show that only one large peak is present at 9.159 E. This peak is associated with the 5.159 E major flutter mode in the strain-gage spectra and, therefore, the flutter mode can be described as a four-nodal-diameter forward traveling wave. (From Eq. (3), the frequency shift in a stationary frame is $\omega_r i$. Thus, $\omega_f/\omega_r + i = 9.159$, and for $\omega_f/\omega_r = 5.159$, $i = 4$.) The tangential displacements in Figs. 5-7 and subsequent figures are expressed in digitized units for convenience. For the main flutter mode, the displacements are also reported in a parametric form.

The correlation of the remaining peaks in the strain-gage and the blade-displacement spectra is based on several observations. First, considering the significant differences in frequencies for the modes in the 14-16E band (compare Figs. 2 and 3 with Fig. 4), one would suspect that this band is a single-blade response, most likely associated with the flow separation. Second, there was a lack of precise synchronization between the strain-gage and displacement-signal tapes. (As mentioned previously, this syncronization was lost at the expense of increased resolution of blade deflections.) Third, the frequencies for the major peaks in the 14-16E range in the strain-gage spectra shifted somewhat with time; however, no such shifts were observed for the other nonintegral order peaks.

It seemed best, therefore, to (1) exclude from consideration the response in the 14-16E range, (2) attempt to associate all other nonintegral order peaks in the strain-gage and the displacement spectra, and (3) attribute the remainder of the response in the displacement spectra to the 14-16E mode. For the relatively low deflections it is important not to overlook the lower modes corresponding to low stress levels (such as peaks at 1.219, 2.031, 3.507, 5.260 and 5.409 E in the strain-gage spectra) because, in general, for a given stress level, a lower mode generates higher deflections than does a higher mode. (Note that the first peak, at 0.406 E, in Figs. 2 and 4 is 60-Hz noise.) When associating different peaks in the two spectra it is also necessary to consider the complements of fractional parts of nonintegral order peaks. These appear in the overall-displacement spectra when a strain-gage frequency, expressed in E's, plus or minus the corresponding nodal diameter is outside the range [0,N/2]. Thus, frequencies associated with these peaks are folded frequencies.

For the major flutter mode (corresponding to the strain-gage frequency of 5.159 E), a slight mistuning was present as shown by the presence of peaks at 1.159 E (Figs. 5 and 6) and 13.159 E (Figs. 5 and 7). Aside from this family, the most noticable peaks are at 10.406 and 0.319 E (Fig. 5) and at 0.478, 0.869, 2.362, 2.782, 4.971, 5.261, and 11.087 E (Fig. 7). These figures include frequencies corresponding to each peak and frequencies (in parentheses) of the associated peaks in the strain-gage spectra. (Note that peaks at 2.782 and 4.971 correspond to nodal diameters -5 and -7; hence, the fractional parts of these frequencies are complements of the fractional parts of the associated strain-gage frequencies.) The peaks at 0.478, 0.869, 2.362, and 11.087 E could not be associated with any peaks singled out in the strain-gage spectra, including the strong peaks in the 14-16E band.

Individual Blade Spectra

The leading-edge blade-deflection spectra for blades 3, 26, and 17, for which the strain-gage spectra are also available (Figs. 2-4), are presented in Fig. 8. In this figure the frequency is folded in the range 0-1/2 E. Aside from the response at 0.159 E, which is associated with the major flutter mode, the highest peak in Fig. 8, blade 3, is at 0.319 E. A peak at the same frequency was noted in the overall blade-displacement spectrum (Fig. 5) and it was associated with the 10.319 E mode in the strain-gage spectra. The peak at 0.493 E, blade 17, is attributed to 3.507 E mode in the strain-gage spectra. However, aside from the these two peaks, significant amplitudes are present (Fig. 8) for blades 3, 26, and 17 at many frequencies as can be seen by comparing their spectra with the spectrum for a relatively quiet blade 30 or by comparing with the midchord port spectra (Fig. 9).

The peaks at 0.087, 0.130, and 0.362 E in Fig. 8, blade 3, can be associated with those at 11.087, 0.869, and 2.362 E in the overall spectrum (Fig. 7). The peaks at 0.014, 0.188, and 0.348 E in the spectrum for this blade and the peak at 0.434 E in the spectrum for blade 17 do not seem to be related to any peaks noted in Figs. 2-7. However, the peak at 0.174 E, blade 17, may be associated with the 15.21 response in the 14-16E band in Fig. 4.

The displacement spectra for the trailing-edge port for blades 3, 26, and 17 are given in Fig. 10. Most of the peaks noted in the strain-gage spectra do appear to be associated with the more visible peaks in these spectra. Moreover, most of the peaks singled out in the overall spectra also appear in Fig. 10. However, the peaks at 0.014, 0.290, and 0.304 E, blade 26, do not seem to be related to any in the strain-gage or the overall spectra. Possibly the last two peaks may be related to the 14.70 E peak in Fig. 3.

In Fig. 10, the peak at 0.217 E, blade 26, is higher than the one at the folded major flutter frequency

0.159 E. A similar situation exists, for example, for blade 1 (Fig. 11) where the peak at 0.130 E is almost as high as the one at 0.159 E. The responses at 0.130 and 0.217 E are associated with those at 0.869 and 2.782 E in the overall spectra. As already noted, the first one, 0.869 E, is not related to any of the responses singled out in the strain-gage spectra. Had blade 1 been strain gaged, it is possible that the source mode for this deflection could be found. However, even without resolving all the details, if the spectra in Fig. 10 or 11 were available during the run they would give a better warning as to the presence of secondary excitations (i.e., not at 0.159 E) than the overall displacement spectra. Another blade for which these secondary excitations were very pronounced was blade 16 (Fig. 11).

Discussion of Spectral Results

The most significant nonintegral response peaks outside the 14-16E range in the tip strain-gage spectra can be related to the distinct peaks in the individual blade spectra for either the leading- or the trailing-edge ports. The majority of these peaks can also be associated with the more visible one in the overall displacement spectra. Of the remaining peaks in the overall spectra, none could be related to the more significant peaks in the 14-16E band in the strain-gage spectra.

Possibly three of the distinct peaks in the individual blade-displacement spectra are related to the strain-gage response in the 14-16E band. However, one of the most striking characterisics of the individual blade spectra is the presence of significant displacement throughout the 0-1/2 E range. This characteristic was observed for most blades, especially the trailing edge. In the absence of any other broad band response, one is led to attribute this characteristic to the 14-16E response in the strain-gage spectra.

This observation has important implications for flutter monitoring, and it points out the need for on-line spectral analysis. Only with the spectral analysis is it possible to determine whether the blade displacement response corresponds to a single frequency, a multitude of frequencies, or a combination of both. In the region close to stall, the broad band of relatively low-level response in the individual blade-deflection spectra is likely to be associated with a single blade response at a high frequency and a significant stress level. To detect this condition it is important to establish the noise floor level during the operation away from instability.

In order to explain the lack of response in the displacement spectra for the 14-16E band and the 10.319E mode, it is desirable to obtain estimates for the deflections corresponding to these modes for the observed stress levels measured by the strain gages. These estimates were obtained by the engine manufacturer by using a finite element code (NASTRAN). The stress levels at the blade-tip strain gage were assumed to be 9.65 MPa (1.4 kpsi) for the chordwise bending mode and 6.89 MPa (1 kpsi) for the second bending mode (Figs. 2-4). (The strain gage was aligned in the direction of the chord near the blade tip 31 percent of the chord from the leading edge.) The corresponding tangential deflections at the leading-edge optical port (located 16 percent of the chord from the leading edge) were 0.1 and 0.77 digital units. (The computed frequencies for these two modes were 2165 and 1332 Hz, respectively; the corresponding frequencies measured in the laboratory on a single blade were 2300 and 1500 Hz; and the associated frequencies measured during engine test were 2140-2270 and 1524 Hz.)

These results offer, therefore, a plausible explanation for the lack of response in the displacement spectra in the 2140-2270 Hz (i.e., 14-16E) range and also for the observed trace response at 0.319 E (which is associated with 10.319 E mode) in Fig. 5. The displacement for this mode is considerably higher for blade 3, Fig. 8. However, this can be attributed to the blade-to-blade amplitude variation. The displacements in Fig. 5 can be viewed as blade-ensemble averages. Hence, they are preferred over the particular values obtained from individual spectra.

Main Flutter Mode

The amplitudes for each blade for the main flutter mode (i.e., corresponding to the frequency of 0.159 E in the individual blade spectra) are presented in Fig. 12; the associated phase angles are shown in Fig. 13. On the whole, the amplitudes appear to be fairly uniform, and the phase angles clearly show the presence of a four-nodal-diameter forward traveling wave. Some of the departures from the constancy of amplitudes (Fig. 12) and slopes (Fig. 13) are undoubtedly caused by a slight mistuning (see Figs. 5-7); however, some of the variations may be caused by inaccuracies associated with the occasional poor peak separation in the folded frequency range 0-1/2 E. This is particularly likely at the trailing edge.

As already indicated, flutter was associated with the second coupled mode. Thus, both bending and torsional deflections can be expected during flutter. In an attempt to separate these two contributions, the total deformations measured perpendicular to the chord are expressed as follows:

$$A_\ell e^{j\phi_\ell} = -r_\ell A_\theta e^{j\phi_\theta} + A_h e^{j\phi_h} \tag{4}$$

$$A_m e^{j\phi_m} = (a - r_\ell) A_\theta e^{j\phi_\theta} + A_h e^{j\phi_h} \tag{5}$$

$$A_t e^{j\phi_t} = (2a - r_\ell) A_\theta e^{j\phi_\theta} + A_h e^{j\theta_h} \tag{6}$$

The total deformations are actually measured in the tangential direction. The following relationships are used to obtain the deformations perpendicular to the chord:

$$\theta = (d_\theta \sin\gamma)/r_\ell$$
$$h = d_h \sin\gamma \tag{7}$$

The left sides of Eqs. (4) to (6) can be considered known. They are obtained from the overall spectra by applying corrections to the phase angles to take into account the fact that optical displacements at the three ports are not measured simultaneously. After these corrections are applied, the phase angles are referenced to the time the once-per-revolution pulse is triggered to begin data acquisition. The variables A_θ, ϕ_θ, A_h, ϕ_h, and r_ℓ are the unknowns. Note, however, that r_ℓ appears only in the combination $r_\ell A_\theta e^{j\phi_\theta}$, which is not independent of $A_h e^{j\phi_h}$. Thus,

although A_θ and ϕ_θ can be determined, additional input is required to determine A_h, ϕ_h, and r_t. Therefore, an assumption was made that the position of the torsional axis (specified by r_t) corresponds to the nodal line position in a single-blade hologram for the above-shroud first torsional mode. (The single-blade holograms were supplied by the engine manufacturer.)

Since there are now two complex unknowns ($A_\theta e^{j\phi_\theta}$ and $A_j e^{j\phi_h}$) and three complex equations, one equation is redundant. If the first two equations (corresponding to the leading edge and the midchord ports) are used, the following set of values are obtained: $r_t A_\theta = 4.15$, $\phi_\theta = 113°$, $A_h = 3.19$, and $\phi_h = -179°$. Because $r_t A_\theta$ and A_h displacements are small, it is convenient to express them in digitized units where one of these units corresponds to a displacement perpendicular to the blade chord of 0.0704 mm. If the first and the third equations (corresponding to the leading and trailing-edge ports) are used $r_t A_\theta = 3.70$, $\phi_\theta = 100°$, $A_h = 2.20$, and $\phi_h = -175°$. These are fairly close to the previously obtained values except for A_h. Thus, blade deformation appears to be somewhat more complicated than assumed in the previous simple model. The main trend is that the bending amplitude is smaller at the trailing edge than at the leading edge. (Note that the same trend would follow had the second and the third equations been solved instead of the first and the third.)

If the average of the previous two sets of values is used, the phase difference $\phi_\theta - \phi_h = -76.5°$ and the coupled flutter parameter (7) $cA_\theta/A_h = 3.52$. Note that the phase difference $\phi_\theta - \phi_h$ depends on the definitions of ϕ and h (Fig. 1).

To get some idea about the accuracy with which the complex torsional and bending displacement components could be determined, another segment of data was digitized at a slower speed (Q = 8860) and the described procedure was then repeated. The amplitudes $r_t A_\theta$ and A_h and the phase difference $\phi_\theta - \phi_h$ were again determined using two sets of equations. This allowed the comparison of four pairs of amplitudes and two pairs of phase angles. The maximum deviation for amplitudes was 8 percent and for the differential phase it was 2°.

CONCLUDING REMARKS

A complex stall-flutter mode can be reasonably resolved into its principal bending and torsional contributions using casing-mounted optical displacement sensors. For the chosen bending and torsional displacement definitions, bending leads torsional displacement by 76° and the coupled flutter parameter (cA_θ/A_h) is 3.52.

Detecting a nonintegral engine order excitation in the blade displacement spectra for higher modes was difficult. The difficulty was compounded by the presence of a wideband response near the chordwise bending mode. The lack of blade to blade coherence for this excitation indicates the lack of coupling between the blades (i.e., single-blade response). Such wideband high-frequency instability generates a response at virtually every frequency line in the folded individual blade spectra. Its recognition, therefore, requires that a noise-floor level be established during the operation away from instability.

The implementaion of the online spectral analysis is essential when using optical sensors for vibration monitoring.

REFERENCES

1 Whitehead, D.S., "Torsional Flutter of Unstalled Cascade Blades at Zero Deflection," Reports and Memoranda No. 3429, Aeronautical Research Council, Great Britain, 1966.

2 Nieberding, W.C., and Pollack, J.L., "Optical Detection of Blade Flutter," ASME Paper No. 77-GT-66, Mar. 1977.

3 Kurkov, A. and Dicus, J., "Synthesis of Blade Flutter Vibratory Patterns Using Stationary Transducers," ASME Paper 78-GT-160, Apr. 1978.

4 Kurkov, A.P., "Flutter Spectral Measurements Using Stationary Pressure Transducers," Journal of Engineering for Power, Vol. 103, No.2, Apr. 1981, pp. 461-467.

5 Kurkov, A.P., "Measurement of Aerodynamic Work During Fan Fluter," Fluid/Structure Interaction in Turbomachinery, American Society of Mechanical Engineers, New York, 1981, pp. 9-18.

6 Singleton, R.C., "An Algorithm for Computing the Mixed Radix Fast Fourier Transform," IEEE Transactions on Audio and Electroacoustics, Vol. AU-17, No.2, June 1969.

7 Halliwell, D.G., "Fan Supersonic Flutter: Prediction and Test Analysis," Aeronautical Research Council R.a M. No. 3789, 1977.

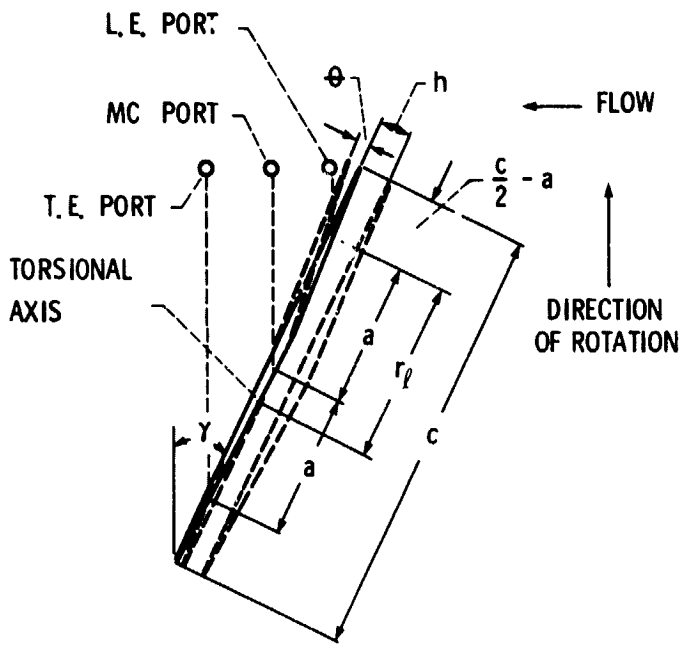

Figure 1. Locations of measurement ports relative to a blade.

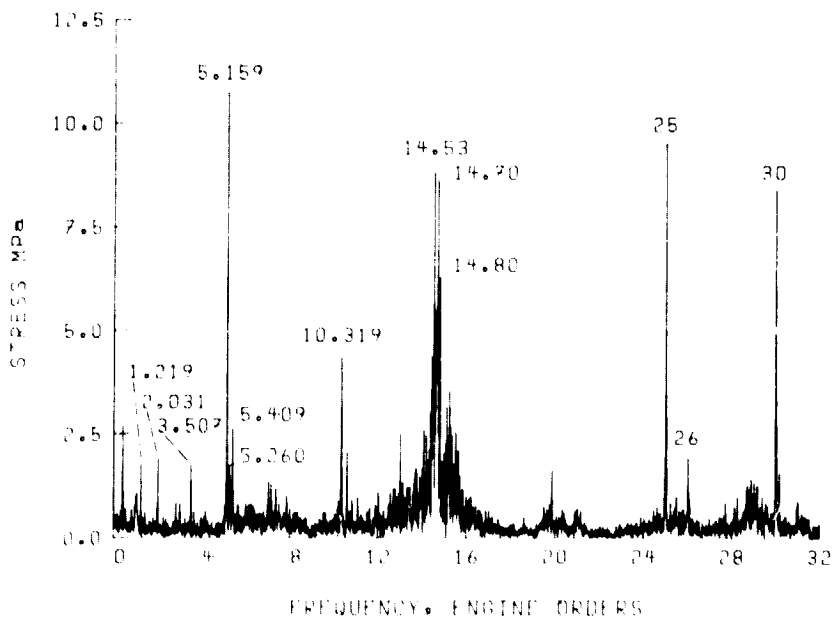

Figure 2. - Strain gage spectrum, blade 3.

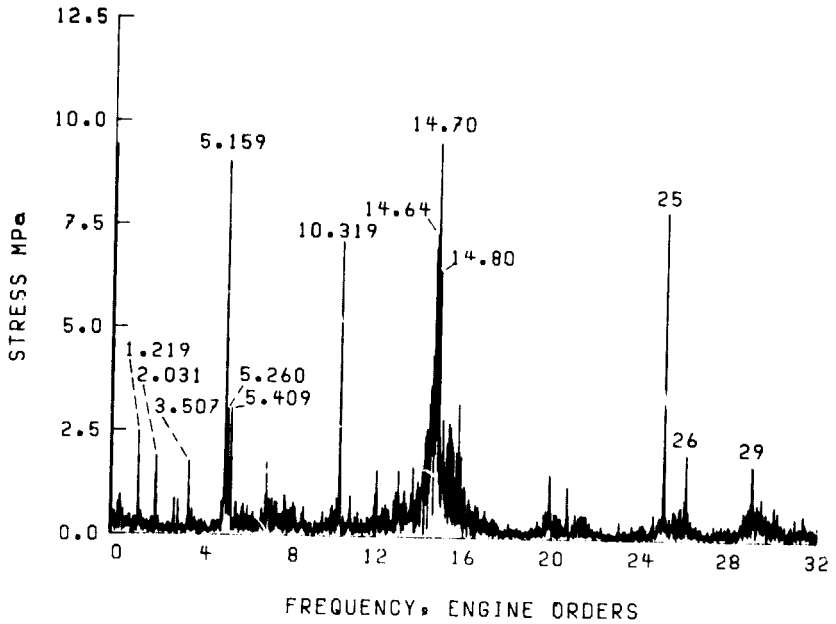

Figure 3. - Strain gage spectrum, blade 26.

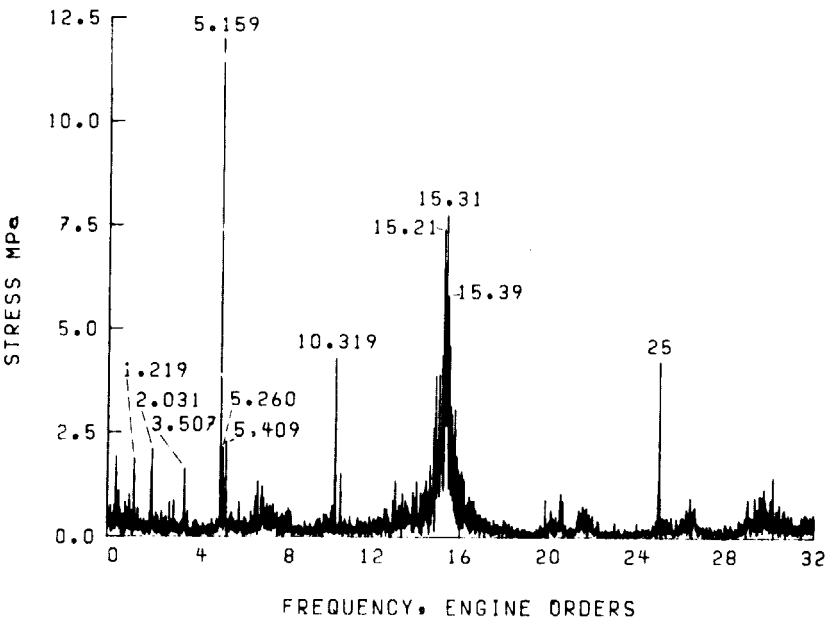

Figure 4. - Strain gage spectrum, blade 17.

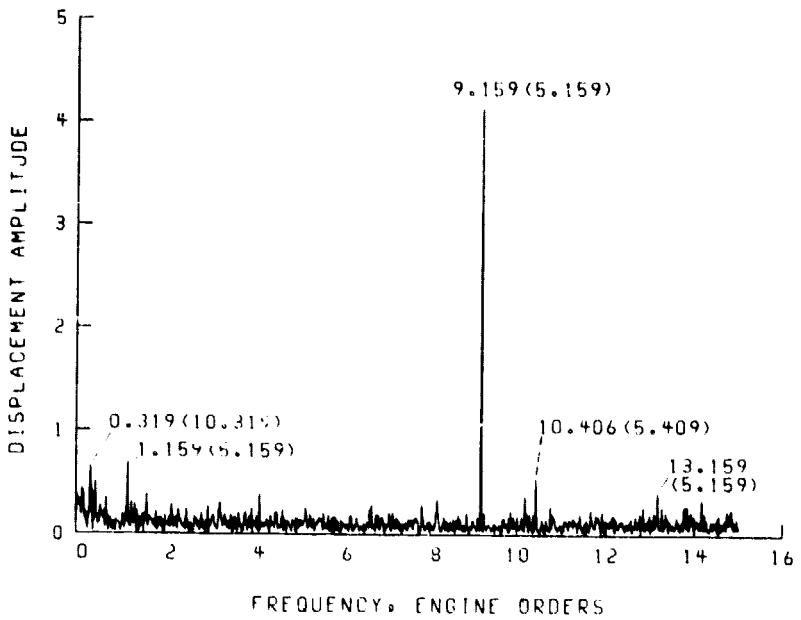

Figure 5. - Overall displacement spectrum, leading edge port. Frequencies in paranthesis correspond to associated peaks in the strain-gage spectra.

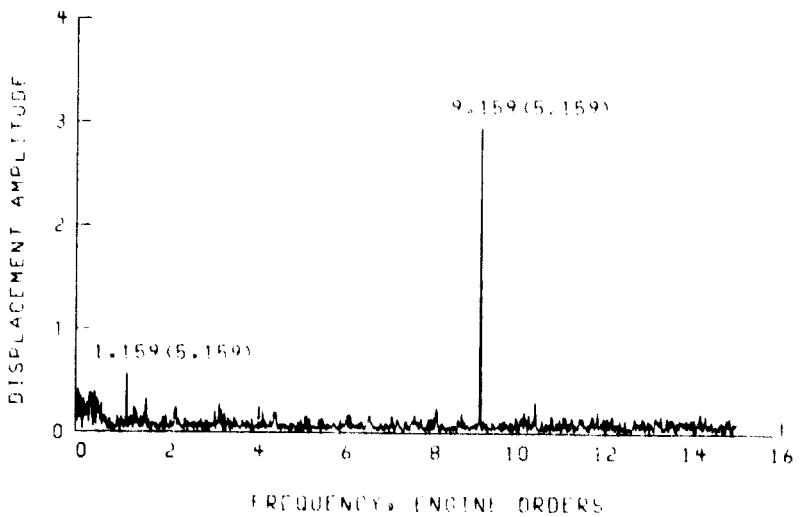

Figure 6. - Overall displacement spectrum, midchord port

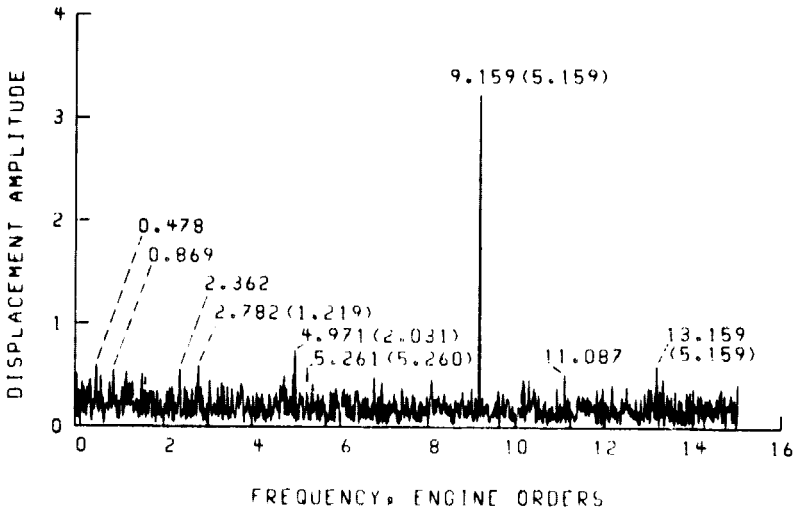

Figure 7. - Overall displacement spectrum, trailing edge port.

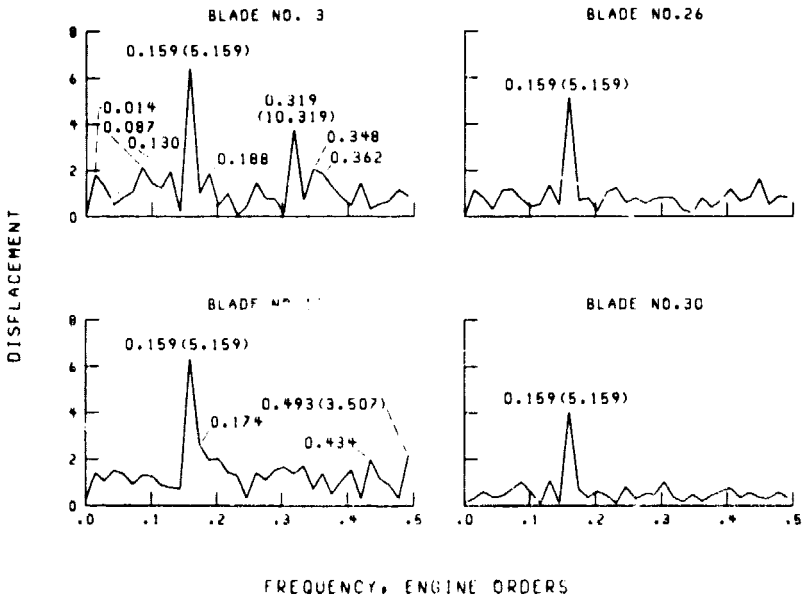

Figure 8. - Displacement spectrum, leading edge port

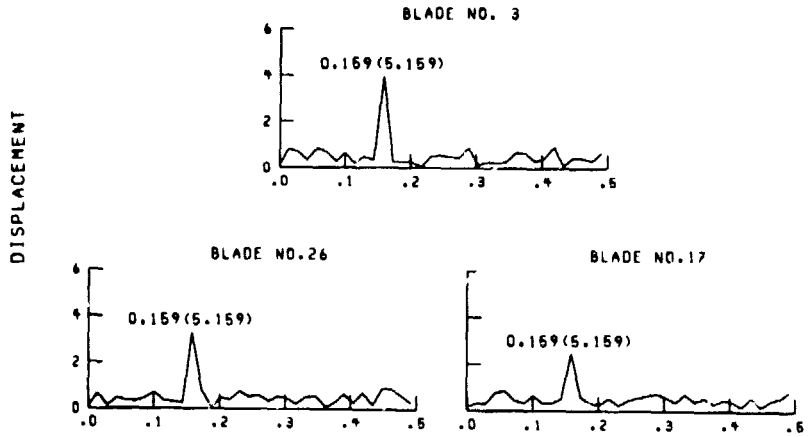

Figure 9. - Displacement spectrum, midchord port

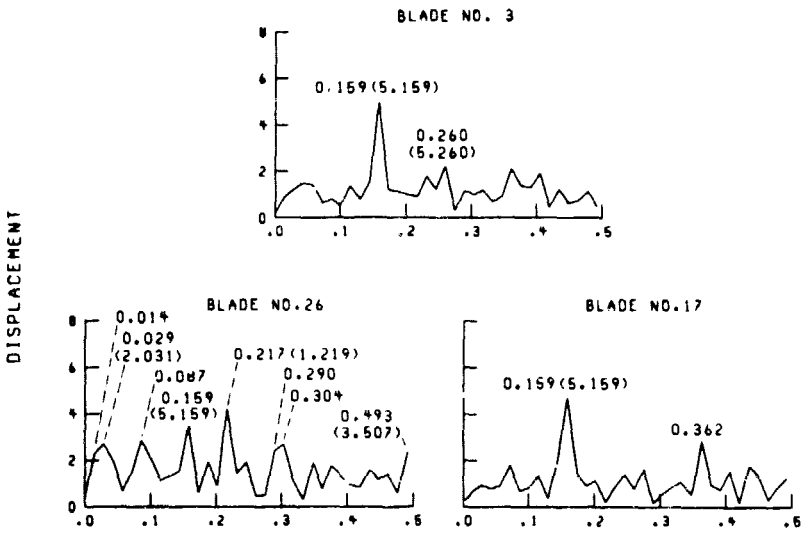

Figure 10. - Displacement spectrum, trailing edge port

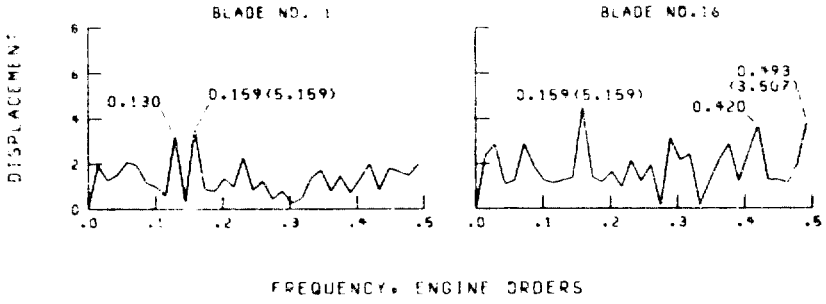

Figure 11. - Displacement spectrum, trailing edge port, blades 1 and 16

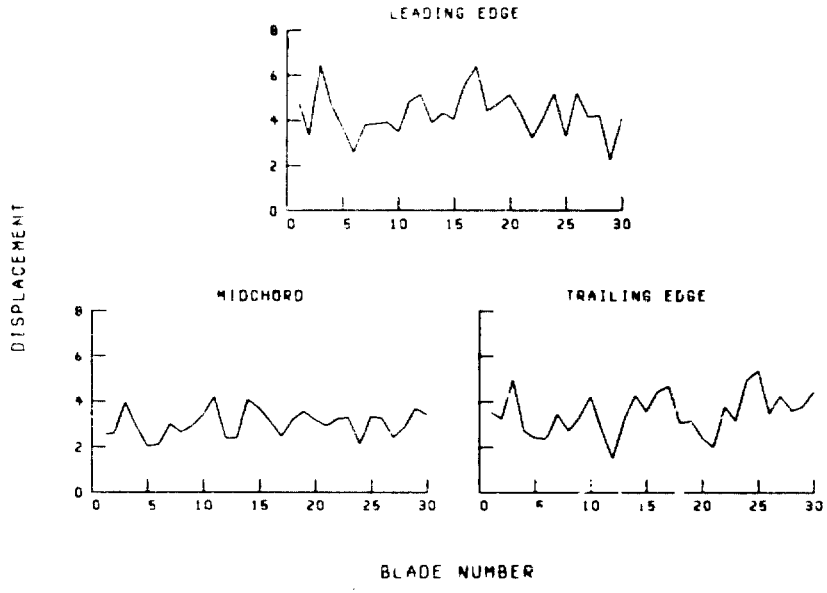

Figure 12. - Displacement amplitudes for the main flutter mode

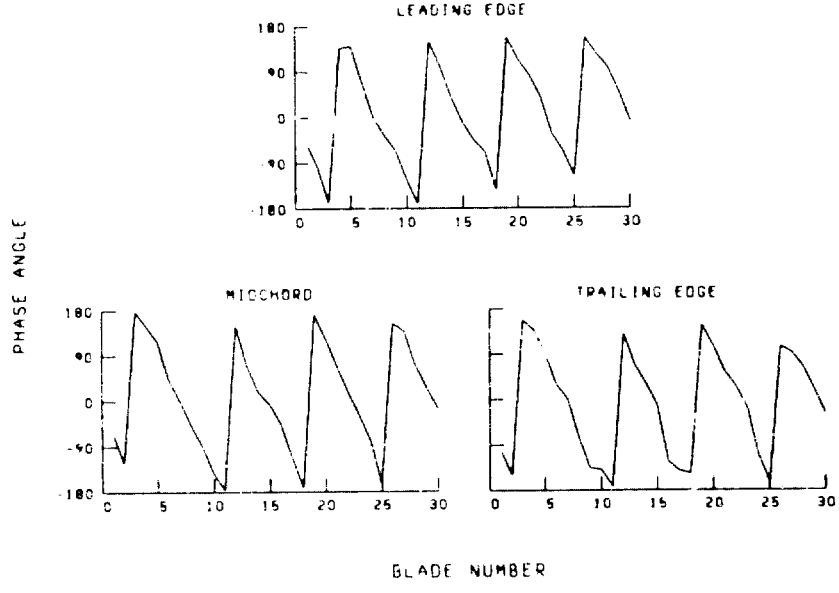

Figure 13. - Displacement phase angles for the main flutter mode